Title

Atomic-Scale Imaging of Condensed Counterions

Authors

Seidler, Morgan
Yu, Tianyi
Luo, Xubo
et al.

Publication Date

2024-10-25

DOI

10.1021/acs.macromol.4c01417

Peer reviewed

Atomic-Scale Imaging of Condensed Counterions

Morgan Seidler[1,2], Tianyi Yu[3], Xubo Luo[3], David Prendergast[3], Ronald N. Zuckermann[3], Nitash P. Balsara[1,2], and Xi Jiang[1]**

1. Materials Sciences Division, Lawrence Berkeley National Laboratory, Berkeley, CA 94720, USA

2. Department of Chemical and Biomolecular Engineering, University of California, Berkeley, CA 94720, USA

3. Molecular Foundry, Lawrence Berkeley National Laboratory, Berkeley, CA 94720, USA

* Corresponding author: xijiang@lbl.gov; nbalsara@berkeley.edu

Table of Contents figure

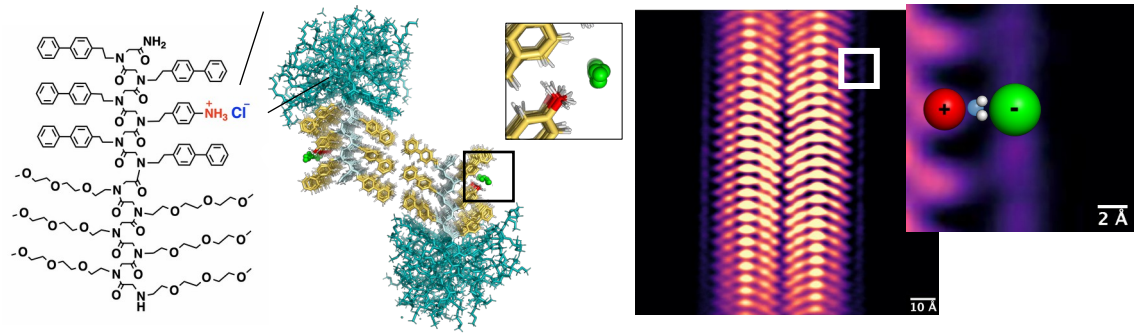

Abstract

The functioning of wide variety of charged macromolecules, from DNA to fuel cell membranes, is dependent on how the counterions surrounding them are arranged. In order to decrease coulombic repulsion, some of the fixed charges on these molecules are neutralized by a fraction of the counterions – this phenomenon is called counterion condensation. The nature of counterion condensation can be only be inferred indirectly from traditional experiments such as X-ray scattering and modern experiments such as single molecule electrometry. The prevalent

conclusion in the literature, based on both theory and experiment, is that the distribution of counterions is peaked right next to the macromolecule, *i.e.*, condensation results in the formation of contact ion pairs. In this study, cryogenic electron microscopy (cryo-EM) was used to study the arrangement of condensed halide counterions near a positively charged polypeptoid nanofiber. The locations of both condensed and fixed charges were determined directly from atomic-scale images. Our experimentally determined counterion distributions were peaked at distances of about 5 Å away from the fixed positive charge, indicating the presence of a layer of water molecules between condensed ion pairs. We posit that this distribution is driven by the entropy of the condensed ions.

Introduction

There has been a long standing interest in the properties of aqueous solutions of charged macromolecules due to their importance in both natural and synthetic systems(*1–3*). The functioning of a diverse array of systems, such as nucleic acids(*4–6*), polypeptides(*7*), and proton-exchange fuel cell membranes(*8*), is dependent on counterions. For example, structured DNA complexes collapse into amorphous aggregates when the counterions are removed via electrodialysis(*4*). In a pioneering study, Manning recognized that the coulombic repulsion between fixed charges on the macromolecule can be reduced by the formation of neutralized ion pairs(*1*, *9*, *10*) - the counterions involved in this pairing are referred to as condensed counterions. Counterion condensation has been studied extensively(*5*, *6*, *9*, *11–26*). Traditional experimental approaches for such studies include including osmometry(*22*), potentiometry(*23*), scattering(*24*, *25*), and NMR(*13*, *20*). In a recent study, Ruggeri et al. calculated the distribution of condensed counterions using data obtained by single-molecule electrometry(*26*). The concentration of

condensed counterions was found to be a monotonically decreasing function of distance, consistent with numerous other theoretical and experimental studies(*12*, *13*, *24*, *25*). In this paper, we use atomic-scale images to establish the presence of non-monotonic counterion distribution functions.

Most models of counterion condensation account for the solvent (usually water) using continuum parameters such as the dielectric constant(*1*, *11*, *12*, *19*). However, in their study of the surprising attraction between negatively charged DNA strands, Rau and Parsegian(*5*) concluded that the main reason for the attraction was the presence of "structured water molecules." In contrast, the theoretical model of Grønbech-Jensen et al.(*19*), which ignores the molecular nature of the aqueous medium, predicts that the attraction between DNA strands is due to correlated fluctuations of the condensed counterions on adjacent strands. In principle, direct atomic-scale imaging may shed light on such controversies.

Figure 1 shows a diagram of a nanofiber with fixed charges, condensed counterions in the vicinity of the nanofiber, and dissociated counterions further away from the nanofiber. It is generally assumed that condensed counterions form contact ion pairs as this would effectively neutralize sections of the charged macromolecule. However, the movement of condensed counterions parallel to the charged macromolecule, that is often observed in simulations(*6*, *19*), would be facilitated by the presence of the solvent layer. Entropic driving forces may also result in the inclusion of solvent molecules. Thus far, there is no direct evidence for solvent-separated ion pairs in condensed counterion layers.

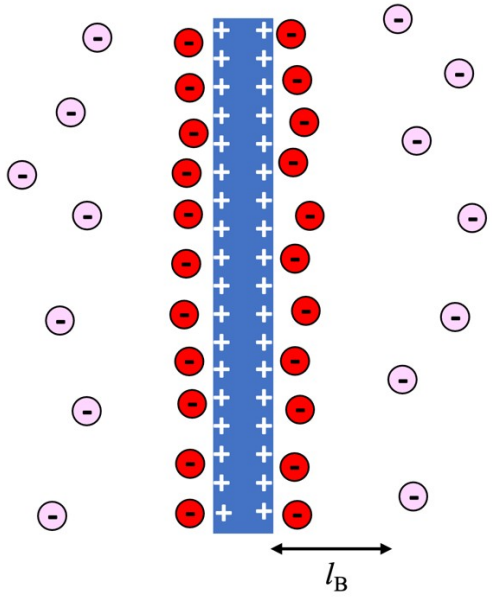

Figure 1. Diagram of a highly charged nanofiber. Diagram of a highly charged nanofiber with fixed positive charges, a layer of condensed counterions near the nanofiber (red), and dissociated counterions (pink) far away. The dissociated counterions are, on average, located at a distance $r > l_B$ away from the nanofiber.

Cryo-EM has been used to image counterions in the vicinity of charged proteins. Previous studies have successfully used cryo-EM to determine the position of bound calcium and chloride ions in the ion cavity(*27–29*). In these studies, the locations of specific counterions in well-defined pockets are determined experimentally. In contrast, we seek to determine the locations of a large collection of counterions. We present images of a charged crystalline nanofiber composed of polypeptoids. Polypeptoids are a class of synthetic polymers with a structure similar to peptides but the side chain is appended to the amide nitrogen instead of the alpha carbon(*30–32*). Amphiphilic diblock copolypeptoids comprising hydrophilic and hydrophobic blocks of equal length were dissolved in water. The ionic groups were located at the ends of the side chains of the hydrophobic block to facilitate the imaging of condensed

counterions. The block copolypeptoids self-assemble into nanofibers. This enables imaging of both the nanofiber with the fixed charge and condensed counterions in the vicinity of the fiber.

Results and Discussion

Diblock copolypeptoids with a hydrophilic (*N*-2-(2-(2-methoxyethoxy)ethoxy) ethylglycine) (Nte) monomer and a hydrophobic (*N*-(2-(4-biphenyl)ethyl)glycine) (NBiPe) monomer were synthesized via a solid-phase synthesis method(*32*). The hydrophobic core of six adjacent monomers at the C-terminus was engineered to contain a single ionic group. Thus, at the ninth monomer from the N-terminus, an aniline-containing monomer *N*-(2-(4-aminophenyl)ethyl)glycine was introduced. The polypeptoid was treated with hydrochloric acid to protonate the amine and form the chloride salt. This polypeptoid is referred to as 9N-Nte_6-$NBipe_6$·Cl. The chemical structure of this polypeptoid is shown in Figure 2(A).

To prepare frozen, hydrated samples, the polypeptoid solution was drop cast on a TEM grid and plunged into liquid ethane(*33*). At this point, the nanofibers are frozen in amorphous ice in their solvated state. We used low-dose imaging procedures developed by the structural biology community to image the nanofibers(*32*, *34*, *35*). One of the images thus obtained is shown in Figure 2(B), where the *a* and *c* crystallographic directions of one of the nanofibers are labeled. These nanofibers are two polypeptoid molecules wide in the *c*-direction, one polypeptoid molecule thick in the *b*-direction, and nearly infinite in the *a*-direction(*32*).

Figure 2(C) is a cartoon of a nanofiber viewed along the long axis of the nanofiber (the *b*-*c* plane). This view, which is orthogonal to the TEM image, clarifies the overall structure of the nanofiber. The hydrophobic NBiPe block crystallizes while the hydrophilic Nte block remains amorphous and extends into the aqueous phase(*32*). The unbound chloride counterions are shown

in green near the positively charged fixed NH_3^+ groups (Figure 2(C)). In the remainder of the paper, we focus on the structure of the nanofiber in the *a*-*c* plane.

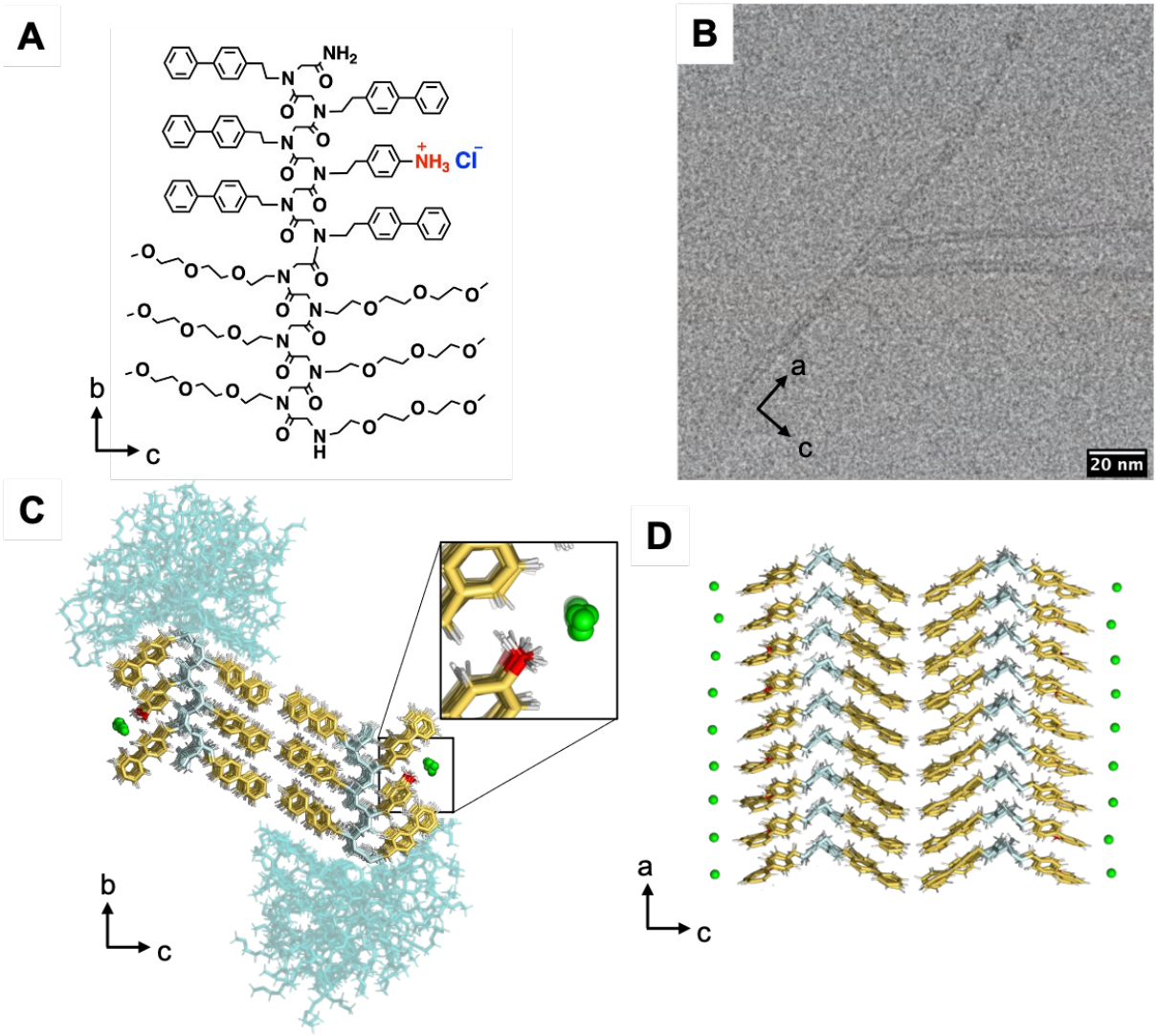

Figure 2. Chemical structure, experimental image and cartoon of nanofibers. The chemical structure of the 9N-Nte$_6$-NBipe$_6$·Cl polypeptoid is shown in panel A. Panel B is a high resolution cryo-EM image of the nanofibers in vitreous ice where the *a* and *c* crystallographic directions are labeled. Panel C is a cartoon of the nanofibers. The inset shows an enlarged view of the bound amine and the unbound chloride counterion. The hydrophilic Nte block (teal) is amorphous and extends into the solvent while the hydrophobic NBipe block (yellow) crystallizes. The yellow

color shows the biphenyl side chains and the white is the polypeptoid backbone. Panel D is a cartoon of the nanofibers oriented in the *a-c* plane, which is the plane seen in the TEM images.

One portion of the self-assembled 9N-Nte_6-$NBipe_6$·Cl nanofiber solution was treated with sodium bicarbonate. The pH of the solution increased from 5.5 to 7.5, thereby neutralizing the amine groups (for reference, the pKa of 4-methylaniline is 5.2(*36*)). The neutral polypeptoid thus obtained is called 9N-Nte_6-$NBipe_6$. A second portion of the self-assembled 9N-Nte_6-$NBipe_6$·Cl nanofiber solution was treated with 100x excess sodium iodide. This procedure exchanges the counterion from chloride to iodide(*37*), and we refer to this polypeptoid as 9N-Nte_6-$NBipe_6$·I.

The 9N-Nte_6-$NBipe_6$·Cl solutions were dominated by nanofibers, while the 9N-Nte_6-$NBipe_6$ and 9N-Nte_6-$NBipe_6$·I solutions contained both nanosheets and nanofibers. The nanosheet morphology is found in a wide variety of amphiphilic block copolypeptoids(*32*, *38*, *39*). We focus on the nanofibers in all three systems. The positions of the nanofibers were identified in the micrographs by Cryosparc(*40*). Then boxes were extracted at those positions, aligned, and averaged into 2D classes. Any classes that contained boxes from nanosheets were filtered out. Figures 3(A), (C), and (E) show the results of this filtering and classification procedure. All three images, which show the crystalline nanofiber in the *a-c* plane, contain two rows of parallel V-shaped motifs. Note that this parallel V-shaped motif in the *a-c* plane is distinct from but consistent with the anti-parallel V-shaped motif in the *b-c* plane. The former shows the crystalline block structure when viewed along the chain backbone while the later shows the orthogonal view of the structure. The brightest spot at the apex of the V represents the glycine backbone while the side chains emanate out to either side. The hydrophobic block of the 9N-Nte_6-$NBipe_6$·Cl polypeptoid is asymmetric (Figure 2(A)). Asymmetry is also seen when one

examines each row in the corresponding image - a band is visible on one side of each row of polypeptoids in Figure 3(A). We posit that this band represents the chloride counterions and that the hydrophilic nature of the $NH_3^+Cl^-$ group drives the ionic side chains toward the aqueous phase. The hydrophobic biphenyl groups without charged groups are driven toward the interior of the nanofiber. Figure 3(B) is a cartoon of the polypeptoid nanofiber where the unbound chloride counterions are placed outside the nanofiber. Figure 3(C) shows an image of the neutralized 9N-Nte_6-$NBipe_6$ polypeptoid. This image does not show bands surrounding the nanofiber, confirming the absence of Cl^- counterions. Consistent with this observation, the corresponding cartoon in Figure 3(D) contains no counterions. Figure 3(E) shows an image of the 9N-Nte_6-$NBipe_6$·I polypeptoid. The bands surrounding the nanofiber confirm the presence of I^- counterions. The electron density within the nanofiber is much higher than that expected from a layer of condensed counterions. Consequently, the images in Figure 3 are dominated by the fiber. The insets in Figure 3(A), (C), and (E) focus on the edge of the fiber. The finger-like structures emanating from the left side represent the edge of the peptoid side chains that form the fiber. A layer of condensed counterions can clearly be seen in Figures 3(A) and (E).

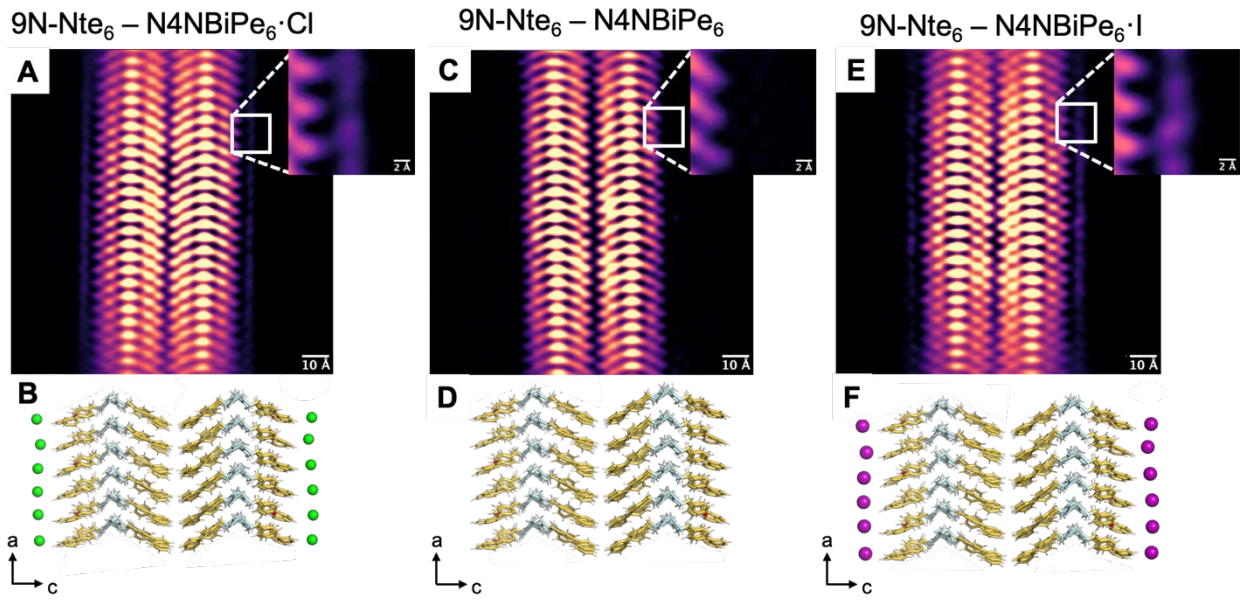

Figure 3. Averaged, high resolution cryo-TEM images of the nanofibers with condensed counterions. Panel A is the experimental cryo-EM image of the 9N-Nte$_6$-NBipe$_6$·Cl nanofibers and the inset shows an enlarged view of the outside of the nanofiber. Panel B is a cartoon of the 9N-Nte$_6$-NBipe$_6$·Cl nanofibers where the chloride ions, in green, are on the outside of the nanofiber. Panel C is the image of the 9N-Nte$_6$-NBipe$_6$ nanofibers, with the cartoon of the fibers is below it in Panel D. Panel E is the image of the 9N-Nte$_6$-NBipe$_6$·I nanofibers with the corresponding cartoon below it. The iodide counterions are shown in purple in Panel F.

While the freezing process does not disrupt the nanofiber, its impact on the location of the counterions remains to be established. Since the importance of coulombic attraction, relative to entropy, increases with decreasing temperature, the counterions may move closer to the nanofiber during the freezing process. In other words, at room temperature the counterions could be further away from the nanofiber than indicated by the TEM images.

The cores of all three nanofibers have a similar lattice structure. However, the characteristic distances between atoms are affected by the chemical composition of the polypeptoid. In Figure 4(A) we show the micrograph of the 9N-Nte$_6$-NBipe$_6$·Cl nanofiber and define three distances – two distances related to the polypeptoid crystalline core and one distance related to the location of the condensed ions. The distances obtained from all three nanofibers are listed in Panel B of Figure 4 (see SI for details). The distance between adjacent polypeptoid molecules along the along the *a* and *c* directions are unaffected by chemical details (*a*-spacing = 4.6 Å ± 0.1 Å and *c*-spacing = 26.4 Å ± 0.5 Å across all three samples). The term ion distance, d_{ion}, is used to quantify the distance between the center of the positively charged nitrogen atom on the amine group and the center of the negatively charged halogen counterions in solution along the *c*-direction. Details concerning the calculation of are given in the supporting information (see discussion related to Figure SI3). The ion distances for 9N-Nte$_6$-NBipe$_6$·Cl and 9N-Nte$_6$-NBipe$_6$·I are 4.7 Å and 5.5 Å, respectively.

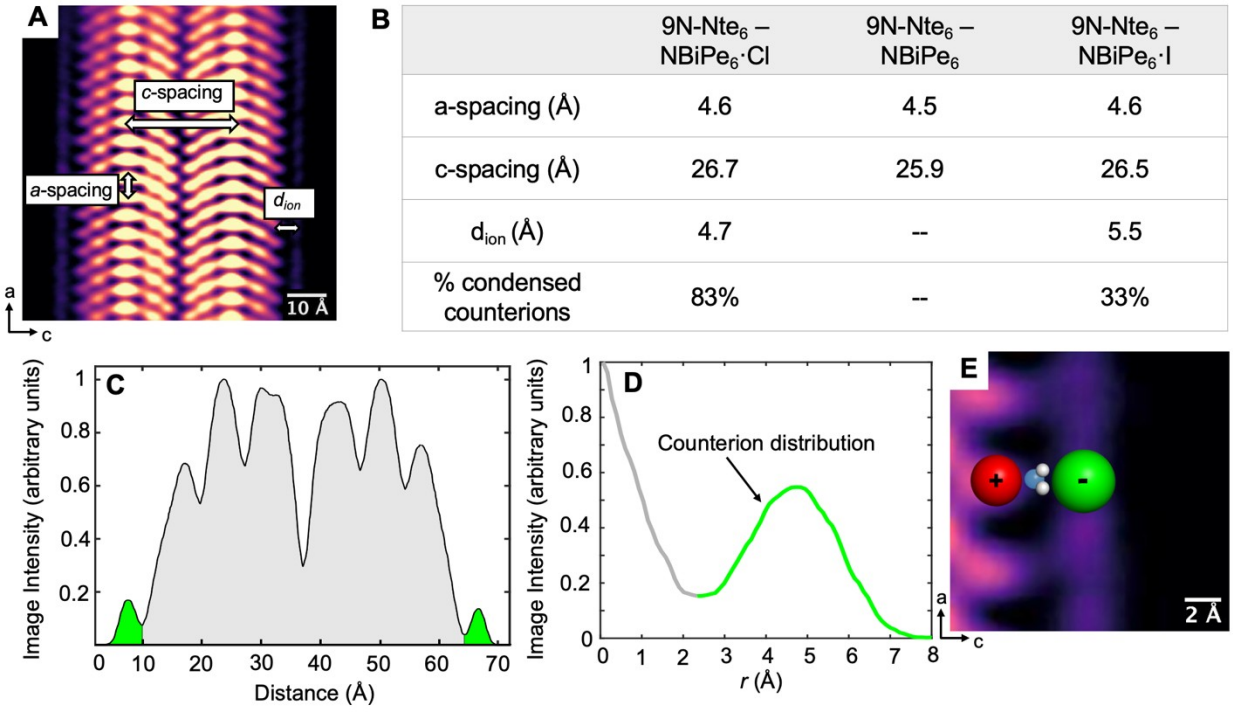

	9N-Nte$_6$ – NBiPe$_6$·Cl	9N-Nte$_6$ – NBiPe$_6$	9N-Nte$_6$ – NBiPe$_6$·I
a-spacing (Å)	4.6	4.5	4.6
c-spacing (Å)	26.7	25.9	26.5
d_{ion} (Å)	4.7	--	5.5
% condensed counterions	83%	--	33%

Figure 4. Measured quantities from high resolution images. Panel A shows the micrograph of 9N-Nte$_6$-NBipe$_6$·Cl and defines the measured lengths. Panel B is a table of the measured lengths of each nanofiber. The error in all distance measurements is ± 0.2 Å (the standard deviation of repeated measurements). Panel C is a line profile of the image in Panel A where average intensity is plotted as a function of distance along the *c* axis. Panel D plots the image intensity versus *r* where *r* is the distance in the *c* direction and *r* = 0 is the position of the positively charged nitrogen bound to the peptoid. Panel E is the inset from Figure 3(A), where the positively charged nitrogen, water molecule, and negatively charged chloride counterion are superimposed over the image. The three species are all drawn to scale.

The distance between fixed charges is 4.6 Å (*a*-spacing) which is less than the Bjerrum length of water, l_B = 7.1 Å(*1*). We therefore expect some fraction of the halide counterions, θ, to be condensed(*1*, *10*). The Manning theory for condensation of univalent ions gives (*10*)

$$\theta = 1 - \frac{a}{l_B} \tag{1}$$

which gives θ = 0.35.

We used the cryo-EM images to obtain an experimental estimate of θ. Figure 4(C) shows image intensity, averaged along the *a* axis versus position along the *c* axis for 9N-Nte$_6$-NBipe$_6$·Cl. The outermost set of peaks in this figure represent the condensed Cl^- counterions while the remainder represents the nanofiber core. If all the Cl^- counterions were condensed and the peptoid monomers were inflexible and in perfect registry, then the ratio of the areas under the Cl-peaks to the core peaks, the A_{Cl}/ A_{core} would be 17/744 = 0.023 (the chloride ion has 17 electrons while the remainder of the 9N-Nte$_6$-NBipe$_6$·Cl has 744 electrons). The measured value of A_{Cl}/

A_{core} is 0.019. Dividing the two values, we obtain a crude estimate for the fraction of condensed counterions, $\theta = 0.83$.

In Figure 4(D), we plot image intensity as a function of position along the *c*-axis, *r*. We define $r = 0$ as the location of the fixed charge. The measured intensity at $r < 2.5$ Å is dominated by nanofiber core. The peak between $r = 2.5$ and 8 Å represents the distribution of condensed counterions. At $r = 8$ Å, a distance that is slightly larger than the Bjerrum length of water, the measured intensity is negligible. We posit that the non-condensed chloride counterions diffuse randomly in the neighborhood of the nanofiber and are thus not detected by averaging-based cryo-EM.

We conducted the same analysis on the 9N-Nte_6-$NBipe_6$·I nanofibers and found results similar to those for chloride counterions. In this case the fraction of condensed counterions, θ, was 0.33 (see Figures S4 and S5), significantly lower than that of 9N-Nte_6-$NBipe_6$·Cl. It is reasonable to assume that a quantitative theory of counterion condensation would include the effect of specific interactions between the counterions and the fixed charges. Because I^- is less electronegative and larger than Cl^-, we expect less counterion condensation in the 9N-Nte_6-$NBipe_6$·I nanofibers(*16*). Given the uncertainties in our quantitative analysis of the cryo-EM data, the quantitative agreement between the value of θ predicted by the Manning theory is probably fortuitous. Nevertheless, the analysis of the cryo-EM data in terms of θ establishes that the contrast between the counterion layers and the polypeptoid nanofiber in Figures 4 and S4 is consistent with that expected from condensed chloride and iodide ions.

In both charged nanofibers, the distance between the fixed and condensed counterions is in the vicinity of 5 Å. This is similar to the typical range for the separation between halides and positively charged coordinating atoms in proteins(*41*). The radius of hydration shells of

dissociated chloride and iodide ions in aqueous media are about 4 and 5 Å, respectively, based on computer simulations(*42*, *43*); the hydration shell of Cl^- is shown in Figure 4(E). The distances reported in Figure 4(B) indicate that the condensed Cl^- and I^- counterions and fixed NH_3^+ ions form solvent-separated ion pairs.

Most theories of counterion condensation predict that the ion concentration is peaked at the surface of the charged nanofiber (r = 0)(*12*, *13*, *24*, *25*). While we have not found any predictions of peaks of finite r values for ion pairs with Cl^- or I^-, Heyda and Dzubiella found that solvent-separated pairs were favored in charged peptides with Cs^+ counterions; contact ion pairs were obtained in all other cases studied(*16*). We hope our results will motivate a detailed atomistic study of counterion condensation in peptoid nanofibers.

Conclusions

The properties of aqueous solutions of charged macromolecules depend on the arrangement of condensed counterions. While there have been numerous theories and simulations that quantify the arrangement of counterions(11, 12, 16), their predictions have not yet been tested against atomic-scale images. Cryogenic electron microscopy is a powerful tool for obtaining atomic-scale images of soft materials. However, most of the images in the literature show atoms connected to each other by covalent bonds(27, 29, 31, 44). The presence of well-defined distances between atoms is important because many high resolution cryo-EM approaches require averaging about 10,000 individual images. Prior to our work, it was not clear if condensed counterions clouds could even be detected by averaging-based cryo-EM. We found that the distances between fixed NH_3^+ ions and condensed counterions in our polypeptoid nanofibers were

peaked at distances of 4.7 and 5.5 Å from the fixed charge for chloride and iodide, respectively, indicating the presence of solvent-separated ion pairs. Based on energetics alone, one expects contact ion pairs as they would minimize coulombic repulsion within the charged nanofiber. However, this would also reduce the entropy of the condensed counterions(*45*, *46*). We hypothesize that the formation of solvent-separated ion pairs is due to entropic considerations, and hope that our study will motivate further study of these contributions . Our work opens the door to direct imaging of more complex systems such as pairs of charged nanofibers wherein correlations between adjacent layers of condensed counterions can be studied directly.

Supporting Information

Details on polypeptoid synthesis, cryo-TEM data collection and analysis, and additional polypeptoid characterization information is included.

Acknowledgements

Soft Matter Electron Microscopy Program (KC11BN), supported by the Office of Science, Office of Basic Energy Science, US Department of Energy, under Contract DE-AC02-05CH11231. M.S. acknowledges funding from the National Science Foundation Graduate Student Research Fellowship DGE 2146752. Work at the Molecular Foundry was supported by the Office of Science, Office of Basic Energy Sciences, of the U.S. Department of Energy under Contract No. DE-AC02-05CH11231. Micrographs presented here were collected at the Berkeley Bay Area Cryo-EM Facility at the University of California, Berkeley.

References

1. G. S. Manning, Limiting Laws and Counterion Condensation in Polyelectrolyte Solutions I. Colligative Properties. *J Chem Phys* **51**, 924–933 (1969).

2. M. Muthukumar, *Physics of Charged Macromolecules: Synthetic and Biological Systems* (Cambridge University Press, 2023).
3. C. F. Anderson, M. T. Record Jr., Salt-Nucleic Acid Interactions. *Annu. Rev. Phys. Chem* **46**, 657–700 (1995).
4. M. U. Musheev, M. Kanoatov, C. Retif, S. N. Krylov, Stable DNA aggregation by removal of counterions. *Anal Chem* **85**, 10004–10007 (2013).
5. D. C. Rau, V. A. Parsegian, Direct measurement of the intermolecular forces between counterion-condensed DNA double helices. Evidence for long range attractive hydration forces. *Biophys J* **61**, 246–259 (1992).
6. B.-Y. Ha, A. J. Liu, Counterion-mediated attraction between two like-charged rods. *Phys Rev Lett* **79**, 1289–1292 (1997).
7. P. Nietmann, K. Kaub, A. Suchenko, S. Stenz, C. Warnecke, M. K. Balasubramanian, A. Janshoff, Cytosolic actin isoforms form networks with different rheological properties that indicate specific biological function. *Nat Commun* **14** (2023).
8. R. S. Yeo, Ion Clustering and Proton Transport in Nafion Membranes and Its Applications as Solid Polymer Electrolyte. *J Electrochem Soc* **130**, 533–538 (1983).
9. G. S. Manning, Limiting Laws and Counterion Condensation in Polyelectrolyte Solutions IV. The Approach to the Limit and the Extraordinary Stability of the Charge Fraction. *Biophys Chem* **7**, 95–102 (1977).
10. G. S. Manning, J. Ray, Counterion condensation revisited. *J Biomol Struct Dyn* **16**, 461–476 (1998).
11. U. Mohanty, B. W. Ninhamt, I. Oppenheim, Dressed polyions, counterion condensation, and adsorption excess in polyelectrolyte solutions. *Proc. Natl. Acad. Sci. USA* **93**, 4342–4344 (1996).
12. B. O'Shaughnessy, Q. Yang, Manning-Oosawa counterion condensation. *Phys Rev Lett* **94** (2005).
13. K. Huber, U. Scheler, New experiments for the quantification of counterion condensation. *Curr Opin Colloid Interface Sci* **17**, 64–73 (2012).
14. J. W. Klien, B. R. Ware, Direct observation of the transition to counterion condensation. *J Chem Phys* **80**, 1334–1339 (1983).
15. J. Xia, P. L. Dubin, H. A. Havel1, Electrophoretic Light Scattering Study of Counterion Condensation on Polylysine. *Macromolecules* **26**, 6335–6337 (1993).
16. J. Heyda, J. Dzubiella, Ion-specific counterion condensation on charged peptides: Poisson-Boltzmann. *Soft Matter* **8**, 9338–9344 (2012).
17. J. Pleštil, D. Hlavatá, Small-angle scattering from polyelectrolyte solutions. A novel method for studying counterion condensation. *Polymer (Guildf)* **29**, 2216–2220 (1988).
18. U. Böhme, A. Klenge, B. Hänel, U. Scheler, Counterion condensation and effective charge of PAMAM dendrimers. *Polymers (Basel)* **3**, 812–819 (2011).
19. N. Grønbech-Jensen, R. J. Mashl, R. F. Bruinsma, W. M. Gelbart, Counterion-induced attraction between rigid polyelectrolytes. *Phys Rev Lett* **78**, 2477–2480 (1997).
20. U. Böhme, U. Scheler, "Counterion mobility and effective charge of polyelectrolytes in solution" in *Macromolecular Symposia* (2004)vol. 211, pp. 87–92.
21. S. Flock, R. Labarbe, C. Houssier, 23Na NMR study of the effect of organic osmolytes on DNA counterion atmosphere. *Biophys J* **71**, 1519–1529 (1996).

22. J. Blaul, M. Wittemann, M. Ballauff, M. Rehahn, Osmotic coefficient of a synthetic rodlike polyelectrolyte in salt-free solution as a test of the Poisson - Boltzmann cell model. *Journal of Physical Chemistry B* **104**, 7077–7081 (2000).
23. C. Wandrey, D. Hunkeler, U. Wendler, W. Jaeger, Counterion activity of highly charged strong polyelectrolytes. *Macromolecules* **33**, 7136–7143 (2000).
24. M. Ballauff, A. Jusufi, Anomalous small-angle X-ray scattering: Analyzing correlations and fluctuations in polyelectrolytes. *Colloid Polym Sci* **284**, 1303–1311 (2006).
25. J. R. C. van der Maarel, L. C. A. Groot, J. G. Hollander, W. Jesse, M. E. Kuil, J. C. Leyte, L. H. Leyte-Zuiderweg, M. Mandel, J. P. Cotton, G. Jannink, A. Lapp, B. Farago, On the charge distribution in aqueous poly(styrenesulfonic acid) solutions. A small angle neutron scattering study. *Macromolecules* **26**, 7295–7299 (1993).
26. F. Ruggeri, F. Zosel, N. Mutter, M. Rozycka, M. Wojtas, A. Ozyhar, B. Schuler, M. Krishnan, Single-molecule electrometry. *Nat Nanotechnol* **12**, 488–495 (2017).
27. J. D. Walter, M. Sawicka, R. Dutzler, Cryo-EM structures and functional characterization of murine Slc26a9 reveal mechanism of uncoupled chloride transport. *Elife* **8** (2019).
28. Z. Deng, Y. Zhao, J. Feng, J. Zhang, H. Zhao, M. J. Rau, J. A. J. Fitzpatrick, H. Hu, P. Yuan, Cryo-EM structure of a proton-activated chloride channel TMEM206. *Sci Adv* **7**, 5983–6007 (2021).
29. E. Park, E. B. Campbell, R. MacKinnon, Structure of a CLC chloride ion channel by cryo-electron microscopy. *Nature* **541**, 500–505 (2017).
30. B. A. Chan, S. Xuan, A. Li, J. M. Simpson, G. L. Sternhagen, T. Yu, O. A. Darvish, N. Jiang, D. Zhang, Polypeptoid polymers: Synthesis, characterization, and properties. *Biopolymers* **109**, 1–25 (2018).
31. X. Jiang, S. Xuan, J. Kundu, D. Prendergast, R. N. Zuckermann, N. P. Balsara, Effect of processing and end groups on the crystal structure of polypeptoids studied by cryogenic electron microscopy at atomic length scales. *Soft Matter* **15**, 4723–4736 (2019).
32. S. Xuan, X. Jiang, R. K. Spencer, N. K. Li, D. Prendergast, N. P. Balsara, R. N. Zuckermann, Atomic-level engineering and imaging of polypeptoid crystal lattices. *Proc Natl Acad Sci U S A* **116**, 22491–22499 (2019).
33. Y. Cheng, Single-particle Cryo-EM at crystallographic resolution. *Cell* **161**, 450–457 (2015).
34. R. F. Egerton, Control of radiation damage in the TEM. *Ultramicroscopy* **127**, 100–108 (2013).
35. M. Seidler, N. K. Li, X. Luo, S. Xuan, R. N. Zuckermann, N. P. Balsara, D. Prendergast, X. Jiang, Importance of the Positively Charged σ-Hole in Crystal Engineering of Halogenated Polypeptoids. *J Phys Chem B* **126**, 4152–4159 (2022).
36. K. C. Gross, P. G. Seybold, Substituent effects on the physical properties and pKa of aniline. *Int J Quantum Chem* **80**, 1107–1115 (2000).
37. M. Druchok, N. Malikova, A. L. Rollet, V. Vlachy, Counter-ion binding and mobility in the presence of hydrophobic polyions - Combining molecular dynamics simulations and NMR. *AIP Adv* **6** (2016).
38. X. Jiang, D. R. Greer, J. Kundu, C. Ophus, A. M. Minor, D. Prendergast, R. N. Zuckermann, N. P. Balsara, K. H. Downing, Imaging unstained synthetic polymer crystals and defects on atomic length scales using cryogenic electron microscopy. *Macromolecules* **51**, 7794–7799 (2018).

39. R. Kudirka, H. Tran, B. Sanii, K. T. Nam, P. H. Choi, N. Venkateswaran, R. Chen, S. Whitelam, R. N. Zuckermann, Folding of a single-chain, information-rich polypeptoid sequence into a highly ordered nanosheet. *Biopolymers* **96**, 586–595 (2011).
40. A. Punjani, J. L. Rubinstein, D. J. Fleet, M. A. Brubaker, CryoSPARC: Algorithms for rapid unsupervised cryo-EM structure determination. *Nat Methods* **14**, 290–296 (2017).
41. R. K. Skitchenko, D. Usoltsev, M. Uspenskaya, A. V. Kajava, A. Guskov, Census of halide-binding sites in protein structures. *Bioinformatics* **36**, 3064–3071 (2020).
42. A. Bankura, B. Santra, R. A. DiStasio, C. W. Swartz, M. L. Klein, X. Wu, A systematic study of chloride ion solvation in water using van der Waals inclusive hybrid density functional theory. *Mol Phys* **113**, 2842–2854 (2015).
43. J. M. Heuft, E. J. Meijer, Density functional theory based molecular-dynamics study of aqueous iodide solvation. *Journal of Chemical Physics* **123** (2005).
44. J. Tian, S. H. Xie, U. Borucu, S. Lei, Y. Zhang, I. Manners, High-resolution cryo-electron microscopy structure of block copolymer nanofibres with a crystalline core. *Nat Mater* **22**, 786–792 (2023).
45. M. J. Stevens, Bundle Binding in Polyelectrolyte Solutions. *Phys Rev Lett* **82**, 101–104 (1999).
46. W. Essafi, F. Lafuma, C. E. Williams, Structural evidence of charge renormalization in semi-dilute solutions of highly charged polyelectrolytes. *European Physical Journal B* **9**, 261–266 (1999).